DALTON

Mixed Fe/Mo mixed-chalcogenide 'hour-glass' clusters, $[Fe_4Mo(CO)_{14}(\mu_3\text{-}E)_2(\mu_3\text{-}E')_2]$ and $[Fe_3Mo(CO)_{11}(\mu_3\text{-}E)(\mu_3\text{-}E')(\mu\text{-}E'\text{–}E')]$ (E, E′ = S, Se or Te)

Pradeep Mathur,*[a] Perumal Sekar,[a] Arnold L. Rheingold[b] and Louise M. Liable-Sands[b]

[a] *Department of Chemistry, Indian Institute of Technology, Bombay 400 076, India*
[b] *Department of Chemistry, University of Delaware, Newark, Delaware 19716, USA*

The room-temperature reactions of $[Fe_2(CO)_6(\mu\text{-}EE')]$ (EE′ = SeTe, STe, SSe, S_2 or Se_2) with $[Mo(CO)_5(thf)]$ (thf = tetrahydrofuran) yielded two types of mixed-metal, mixed-chalcogenide 'hour-glass' clusters: $[Fe_4Mo(CO)_{14}(\mu_3\text{-}E)_2(\mu_3\text{-}E')_2]$ (E, E′ = Se, Te **1**; S, Te **2**; S, Se **4**; S, S **7**; Se, Se **9**) and $[Fe_3Mo(CO)_{11}(\mu_3\text{-}E)(\mu_3\text{-}E')(\mu\text{-}E'\text{–}E')]$ (E, E′ = S, Te, E′–E′ = Te–Te **3**; E, E′ = S, Se, E′–E′ = Se–Se **5**; E, E′ = S, S, E′–E′ = S–Se **6**; E, E′ = S, S, E′–E′ = S–S **8**; E, E′ = Se, Se, E′–E′ = Se–Se **10**). The crystal structures of **2**, **5**, **6** and **8** were elucidated by X-ray methods. The structure of **2** consists of two distorted square-pyramidal cores in each of which the alternate corners of the base are occupied by Fe and chalcogen atoms and a Mo atom occupies the common apical site. In **5**, **6** and **8** a Mo atom occupies the common apical site of a square-pyramidal core and a tetrahedral core. The base of the square-pyramidal unit consists of alternate Fe and chalcogen atoms and the tetrahedral base consists of a Fe atom and two chalcogen atoms.

Facile addition of co-ordinatively unsaturated transition-metal species to the reactive E–E bonds of $[Fe_2(CO)_6(\mu\text{-}E_2)]$ (E = S, Se or Te) provides a convenient method to obtain numerous chalcogen-bridged mixed-metal carbonyl clusters.[1] The addition of mononuclear carbonyl fragments to form square-pyramidal cluster cores can occur in one of two possible ways: one is accompanied by formation of one new metal–metal bond and the heterometal atom occupies a basal site (**A**), and the other in which two new metal–metal bonds are formed and the heterometal occupies the apical site (**B**).[2–4] Reactions of $[Mo(CO)_5(thf)]$ and $[W(CO)_5(thf)]$ (thf = tetrahydrofuran) with $[Fe_2(CO)_6(\mu\text{-}E_2)]$ to form type B mixed-metal clusters have been found to be dependent on the nature of E in $[Fe_2(CO)_6(\mu\text{-}E_2)]$. When E = Te, $[W(CO)_5(thf)]$ reacts to form $[Fe_2W(CO)_{10}(\mu_3\text{-}Te)_2]$, but there is no reaction of $[Mo(CO)_5(thf)]$. When E = Se both molybdenum and tungsten moieties add to form $[Fe_2M(CO)_{10}(\mu_3\text{-}Se)_2]$ (M = Mo or W) clusters. In order to further investigate the influence of the different chalcogen ligands in mixed-metal cluster syntheses, we have looked at the reactivity of the mixed-chalcogenide compounds $[Fe_2(CO)_6(\mu\text{-}EE')]$ with $[Mo(CO)_5(thf)]$. In a preliminary communication we reported the formation of an unusual 'hour-glass' cluster $[\{Fe_2(CO)_6(\mu_3\text{-}Se)(\mu_3\text{-}Te)\}_2Mo(CO)_2]$ (Fig. 1) from the reaction of $[Fe_2(CO)_6(\mu\text{-}SeTe)]$ with $[Mo(CO)_5(thf)]$.[5] Formation of **1** was thought to proceed *via* initial formation of the square-pyramidal $[Fe_2Mo(CO)_{10}(\mu_3\text{-}Se)(\mu_3\text{-}Te)]$, though the latter could not be isolated.

In continuation of our investigation on the influence of different chalcogen ligands in mixed-metal cluster growth reactions and to understand the mechanism of formation of the hour-glass cluster, we report here the reactions of the mixed chalcogenide $[Fe_2(CO)_6(\mu\text{-}STe)]$ and $[Fe_2(CO)_6(\mu\text{-}SSe)]$ with $[Mo(CO)_5(thf)]$. In order to complete the study on the homochalcogenide series, we have also examined closely the reaction of $[Fe_2(CO)_6(\mu\text{-}S_2)]$ and of $[Fe_2(CO)_6(\mu\text{-}Se_2)]$ with $[Mo(CO)_5(thf)]$ and have isolated two new clusters with hitherto unknown core geometries.

Results and Discussion

Synthesis

When 2 equivalents of $[Fe_2(CO)_6(\mu\text{-}EE')]$ (EE′ = SeTe, STe, SSe, S_2 or Se_2) and a freshly prepared solution of $[Mo(CO)_5(thf)]$ were stirred in hexane–thf solvent at room temperature (r.t.) for 3 h the reaction mixture changed from orange to green and the infrared spectrum indicated some new bands in the CO region. Chromatographic work-up separated two types of clusters from these reaction mixtures: green clusters of the general form $[Fe_4Mo(CO)_{14}(\mu_3\text{-}E)_2(\mu_3\text{-}E')_2]$ (EE′ = SeTe **1**, STe **2**, SSe **4**, S_2 **7** or Se_2 **9**) and the orange clusters $[Fe_3Mo(CO)_{11}(\mu_3\text{-}E)(\mu_3\text{-}E')(\mu\text{-}E'_2)]$ (EE′, E′$_2$: STe, Te_2 **3**; SSe, Se_2 **5**; SS, SSe **6**; SS, S_2 **8**; or SeSe, Se_2 **10**) (Scheme 1). The relative yields of these two types of clusters obtained in each reaction depended on the nature of E and E′ in the reactant, $[Fe_2(CO)_6(\mu\text{-}EE')]$. When the E, E′ combinations in $[Fe_2(CO)_6(\mu\text{-}EE')]$ are Se, Te or S, Te, the green Fe_4Mo cluster is the sole or the major product, respectively, isolated from the reaction mixture. For the other chalcogen combinations the green clusters are minor products and the orange Fe_3Mo clusters are the major products. From the reaction of $[Fe_2(CO)_6(\mu\text{-}SSe)]$ with $[Mo(CO)_5(thf)]$ two orange clusters with different chalcogen combinations were isolated, $[Fe_3Mo(CO)_{11}(\mu_3\text{-}S)(\mu_3\text{-}Se)(\mu\text{-}Se_2)]$ **5** and $[Fe_3Mo(CO)_{11}(\mu_3\text{-}S)_2(\mu\text{-}SSe)]$ **6**. Close monitoring of the reactions by TLC and infra-

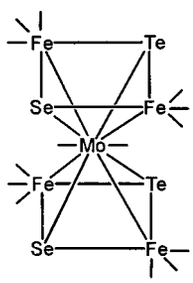

Fig. 1 The structure of $[Fe_4Mo(CO)_{14}(\mu_3\text{-}Se)_2(\mu_3\text{-}Te)_2]$

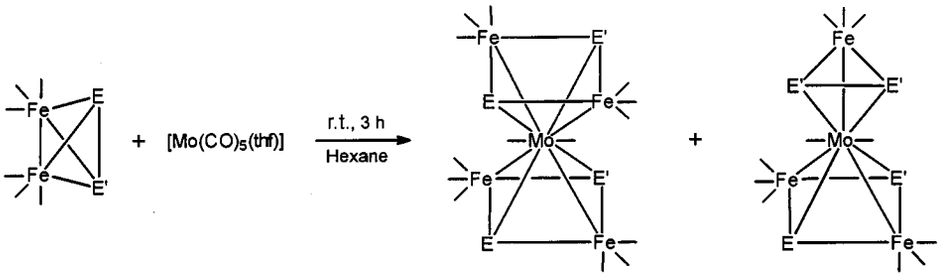

E, E' = Se, Te — **1**. E, E' = Se, Te —

E, E' = S, Te — **2**. E, E' = S, Te — **3**. E, E' = S, Te; E'–E' = Te–Te

E, E' = S, Se — **4**. E, E' = S, Se — **5**. E, E' = S, Se; E'–E' = Se–Se

6. E, E' = S, S; E'–E' = S–Se

E, E' = S, S — **7**. E, E' = S, S — **8**. E, E' = S, S; E'–E' = S–S

E, E' = Se, Se — **9**. E, E' = Se, Se — **10**. E, E' = Se, Se; E'–E' = Se–Se

Scheme 1 Preparation of 'hour-glass' clusters

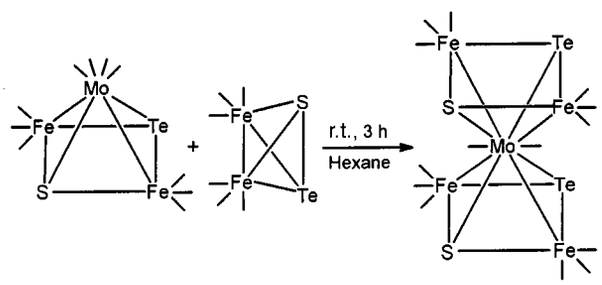

Scheme 2 Conversion of the square-pyramidal $[Fe_2Mo(CO)_{10}(\mu_3\text{-}S)(\mu_3\text{-}Te)]$ into the 'hour-glass' $[Fe_4Mo(CO)_{14}(\mu_3\text{-}S)_2(\mu_3\text{-}Te)_2]$

red spectroscopy indicated that initially a maroon band is formed the infrared spectrum of which shows a carbonyl stretching frequency pattern similar to that observed for the square-pyramidal $[Fe_2Mo(CO)_{10}(\mu_3\text{-}E)(\mu_3\text{-}E')]$ clusters, reported previously.[4] During the course of the reaction the maroon bands gradually faded as the amounts of the green and orange clusters grew. Attempts to isolate pure maroon bands for complete identification proved to be unsuccessful. In most cases, during the chromatography, they converted into the green bands of the Fe_4Mo clusters. In case of the reaction of $[Fe_2(CO)_6(\mu\text{-}STe)]$ with $[Mo(CO)_5(thf)]$ the maroon band was sufficiently stable to enable investigation of its reaction with $[Fe_2(CO)_6(\mu\text{-}STe)]$; on stirring for 3 h at room temperature, almost quantitative formation of the green $[Fe_4Mo(CO)_{14}(\mu_3\text{-}S)_2(\mu_3\text{-}Te)_2]$ **2** was observed (Scheme 2). The green bands **4**, **7** and **9** gradually converted into orange compounds **5**, **8** and **10** during the chromatographic work-up.

Compounds **2**, **5**, **6** and **8** were characterised by IR spectroscopy and their structures established by single-crystal X-ray diffraction analysis; **3**, **4**, **7**, **9** and **10** were identified by comparison of their infrared spectra with those of the structurally characterised analogous compounds **2**, **5** and **8**. The infrared spectra of **2**, **4**, **7** and **8** show the presence of only terminally bonded carbonyl groups with a complex CO stretching pattern similar to that observed for $[Fe_4Mo(CO)_{14}(\mu_3\text{-}Se)_2(\mu_3\text{-}Te)_2]$.[5] The infrared spectra of **3**, **6**, **8** and **10** were similar with an identical CO stretching pattern. There is a regular shift of the corresponding bands to lower ν(CO) values in $[Fe_4Mo(CO)_{14}(\mu_3\text{-}E)_2(\mu_3\text{-}E')_2]$ for the following combination of EE′ ligands: S_2 > SSe > Se_2 > STe > SeTe. Attempts to prepare the tellurium analogue of $[Fe_4Mo(CO)_{14}(\mu_3\text{-}E)_2(\mu_3\text{-}E')_2]$ were unsuccessful. The infrared spectral data for compounds **1**–**10** are given in Table 1.

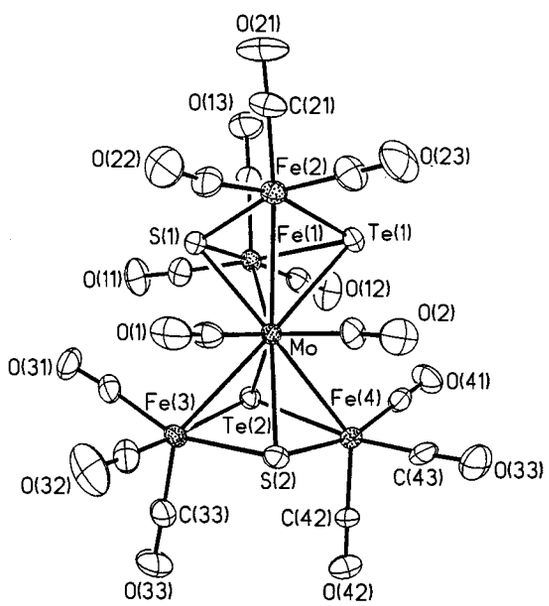

Fig. 2 Molecular structure of compound **2**

Molecular structure of compound 2

Dark red crystals of compound **2** suitable for X-ray diffraction analysis were grown from a hexane–dichloromethane mixture by slow evaporation of the solvents at −5 °C and an X-ray diffraction study was undertaken. An ORTEP[6] diagram of the molecular structure of **2** is shown in Fig. 2. The Mo atom occupies the common apical site of two distorted square-pyramidal cores, in each of which the two Fe atoms, one S atom and one Te atom occupy the basal sites. Two terminally bonded carbonyl ligands on the Mo atom give it an overall co-ordination number of ten. Each Fe atom has three terminal carbonyl groups. Three of the four Mo–Fe bond distances [2.815(2)–2.848(2) Å] (Table 2) are comparable with the Mo–Fe bond lengths reported for other Mo/Fe mixed-metal clusters stabilised by chalcogen ligands, $[\{(C_5H_4Me)MoS_2Fe(CO)_3\}_2]$, 2.853(3) Å,[7] $[MoFeCo(\eta\text{-}C_5H_5)(CO)_7(PMePrPh)(\mu_3\text{-}S)]$, 2.793(2) Å,[8] $[\{(OC)_2MoFeCo(CO)_6(\mu_3\text{-}S)\}_2\{\eta^5\text{-}C_5H_4C(O)CH_2CH_2C(O)C_5H_4\text{-}\eta^5\}]$, 2.801(1) Å,[9] and $[Mo_2Fe_2(\eta\text{-}C_5H_5)_2(CO)_6(\mu_3\text{-}CO)_2(\mu_3\text{-}S)_2]$, 2.816(5) Å,[10] whereas the fourth bond is somewhat long [Mo–Fe(1) 3.052(2) Å], making one of the square pyramids more distorted than the other. While the two Mo–S

Table 1 Preparation of $[Fe_4Mo(CO)_{14}(\mu_3\text{-}E)_2(\mu_3\text{-}E')_2]$ (E = S or Se; E′ = S, Se or Te) and $[Fe_3Mo(CO)_{11}(\mu_3\text{-}E)(\mu_3\text{-}E')(\mu\text{-}E'_2)]$ (E = S; E′ = Se or Te; E = E′ = S or Se)

Amount used/g (mmol)					Carbon analysis[a]	
$[Fe_2(CO)_6(\mu\text{-}EE')]$	$[Mo(CO)_6]$	Product	Yield/g (%)	IR ($\tilde{\nu}_{CO}$/cm^{-1}, hexane)	(%)	M.p. (°C)[b]
$[Fe_2(CO)_6(\mu\text{-}SeTe)]$ 0.25 (0.51)	0.068 (0.26)	$[Fe_4Mo(CO)_{14}(\mu_3\text{-}Se)_2(\mu_3\text{-}Te)_2]$ **1**	0.053 (31)	2083w, 2057vs, 2050vs, 2043vs, 2019w, 2009s, 1996w, 1989w, 1982w	15.3 (15.0)	174–176
$[Fe_2(CO)_6(\mu\text{-}STe)]$ 0.5 (1.14)	0.15 (0.57)	$[Fe_4Mo(CO)_{14}(\mu_3\text{-}S)_2(\mu_3\text{-}Te)_2]$ **2**	0.31 (40)	2087w, 2061vs, 2053vs, 2046vs, 2026w, 2022w, 2013s, 1999w, 1993w, 1984w	16.5 (16.3)	156–158
		$[Fe_3Mo(CO)_{11}(\mu_3\text{-}S)(\mu_3\text{-}Te)(\mu\text{-}Te_2)]$ **3**	0.11 (14)	2087w, 2064s, 2054vs, 2045vs, 2023w, 2015s, 2003m, 1994w	13.1 (12.7)	147–149
$[Fe_2(CO)_6(\mu\text{-}SSe)]$ 0.4 (1.02)	0.135 (0.51)	$[Fe_4Mo(CO)_{14}(\mu_3\text{-}S)_2(\mu_3\text{-}Se)_2]$ **4**	0.07 (12)	2091w, 2062vs, 2052vs, 2025w, 2015s, 1997w (br)	18.2 (18.0)	146–148
		$[Fe_3Mo(CO)_{11}(\mu_3\text{-}S)(\mu_3\text{-}Se)(\mu\text{-}Se_2)]$ **5**	0.2 (35)	2090w, 2066vs, 2056vs, 2051vs, 2028w, 2016s, 2002w, 1997w	15.0 (14.7)	141–143
		$[Fe_3Mo(CO)_{11}(\mu_3\text{-}S)_2(\mu\text{-}SSe)]$ **6**	0.13 (27)	2093w, 2067vs, 2053vs, 2029w, 2017s, 2005w, 1999w	17.6 (17.7)	134–138
$[Fe_2(CO)_6(\mu\text{-}S_2)]$ 0.5 (1.45)	0.19 (0.72)	$[Fe_4Mo(CO)_{14}(\mu_3\text{-}S)_4]$ **7**	0.035 (5)	2095w, 2069vs, 2057vs, 2053vs, 2033w, 2025w, 2016s, 1998w	*c*	*c*
		$[Fe_3Mo(CO)_{11}(\mu_3\text{-}S)_2(\mu\text{-}S_2)]$ **8**	0.2 (30)	2088w, 2063vs, 2054vs, 2028s, 2017w, 2012w, 2005m	17.7 (17.5)	127–129
$[Fe_2(CO)_6(\mu\text{-}Se_2)]$ 0.5 (1.14)	0.15 (0.57)	$[Fe_4Mo(CO)_{14}(\mu_3\text{-}Se)_4]$ **9**	0.04 (7)	2089w, 2065vs, 2052vs, 2045vs, 2031w, 2013s, 1989w	*c*	*c*
		$[Fe_3Mo(CO)_{11}(\mu_3\text{-}Se)_2(\mu\text{-}Se_2)]$ **10**	0.05 (10)	2090w, 2064vs, 2053vs, 2048vs, 2027s, 2011w, 2005w, 1996w	15.3 (14.9)	145–147

[a] Calculated values in parentheses. [b] With decomposition. [c] Values are not available because of instability of the product.

Table 2 Selected bond lengths (Å) and angles (°) for $[Fe_4Mo(CO)_{14}(\mu_3\text{-}S)_2(\mu_3\text{-}Te)_2]$ **2**

Mo–Fe(1)	3.052(2)	Fe(1)–S(1)	2.286(3)
Mo–Fe(2)	2.815(2)	Fe(2)–S(1)	2.256(3)
Mo–Fe(3)	2.830(2)	Fe(3)–S(2)	2.256(4)
Mo–Fe(4)	2.848(2)	Fe(4)–S(2)	2.244(3)
Mo–S(1)	2.431(3)	Fe(1)–Te(1)	2.572(2)
Mo–S(2)	2.433(3)	Fe(2)–Te(1)	2.558(2)
Mo–Te(1)	2.741(11)	Fe(3)–Te(2)	2.546(2)
Mo–Te(2)	2.798(14)	Fe(4)–Te(2)	2.537(2)
Fe(2)–Mo–Fe(1)	74.7(5)	Te(2)–Mo–Fe(1)	58.9(4)
S(1)–Mo–Fe(1)	47.7(7)	Te(2)–Mo–Fe(2)	133.5(5)
S(1)–Mo–Fe(2)	50.3(8)	Fe(2)–Mo–Fe(3)	138.4(6)
Te(1)–Mo–Fe(1)	52.4(4)	Fe(2)–Mo–Fe(4)	143.3(5)
Te(1)–Mo–Fe(2)	54.8(4)	S(1)–Mo–Fe(3)	94.0(8)
Fe(3)–Mo–Fe(4)	77.6(5)	S(1)–Mo–Fe(4)	142.6(9)
S(2)–Mo–Fe(3)	50.1(8)	Te(1)–Mo–Fe(3)	146.9(9)
S(2)–Mo–Fe(4)	49.5(8)	Te(1)–Mo–Fe(4)	91.4(4)
Te(2)–Mo–Fe(3)	53.8(4)	S(1)–Mo–S(2)	142.9(10)
Te(2)–Mo–Fe(4)	53.4(4)	S(1)–Mo–Te(1)	75.9(7)
Fe(3)–Mo–Fe(1)	97.5(6)	S(1)–Mo–Te(2)	92.1(8)
Fe(4)–Mo–Fe(1)	96.9(5)	S(2)–Mo–Te(1)	138.4(8)
S(2)–Mo–Fe(1)	133.3(9)	S(2)–Mo–Te(2)	74.5(9)
S(2)–Mo–Fe(2)	151.9(10)	Te(1)–Mo–Te(2)	94.6(4)

distances are similar [2.431(3), 2.433(3) Å], there is a considerable difference in the two Mo–Te bond lengths [2.741(11), 2.798(14) Å].

The sulfur and tellurium ligands adopt the μ_3 bridging mode and thereby function as four-electron donors to the cluster. In terms of electron-counting rules, **2** is a 82-electron cluster, and the formal application of the 18-electron rule would predict four metal–metal bonds, as observed.

Molecular structures of compounds 5, 6 and 8

Red plate crystals of compounds **5**, **6** and **8** were grown from their hexane–dichloromethane solvent mixtures at −5 °C and X-ray structural analyses were carried out. The ORTEP diagrams of their molecular structures are shown in Figs. 3–5, selected bong lengths and angles in Tables 3–5. Clusters **5**, **6** and **8** are isomorphous and isostructural, and consist of a Mo atom which occupies the common apical site of square-pyramidal and tetrahedral cores. The square base in **5**, **6** and **8** consists of an alternate arrangement of Fe and chalcogen atoms, whereas the triangular base consists of one Fe and two chalcogen atoms. Two terminally bonded carbonyl ligands on the Mo atom give it

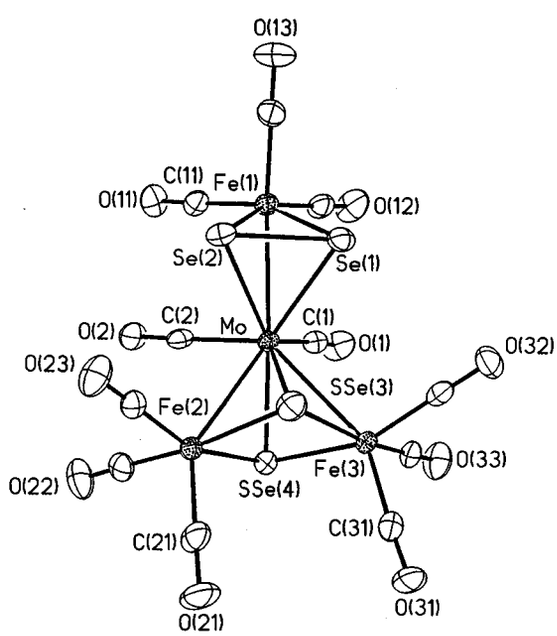

Fig. 3 Molecular structure of compound **5**

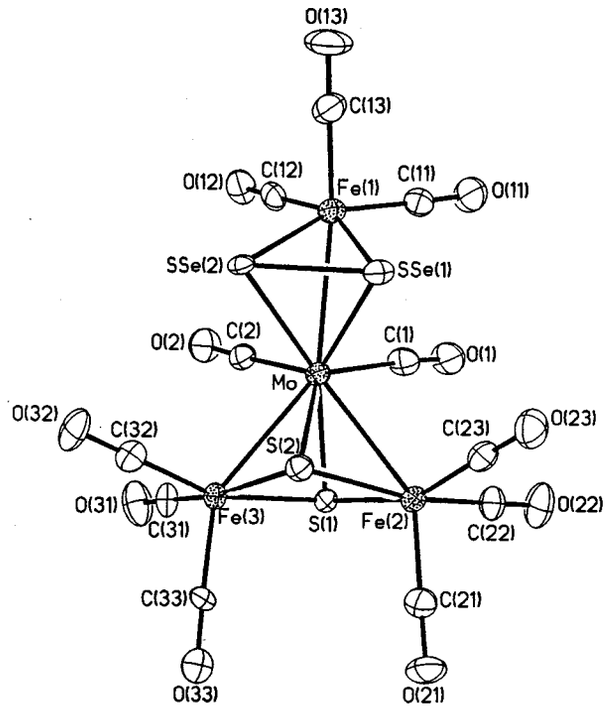

Fig. 4 Molecular structure of compound **6**

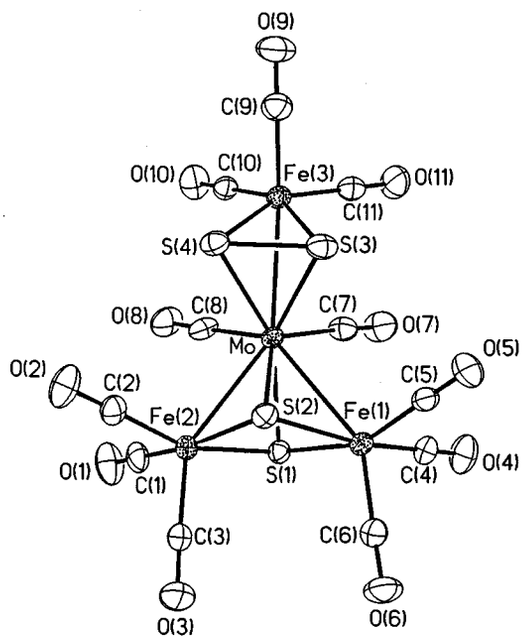

Fig. 5 Molecular structure of compound **8**

an overall co-ordination number of nine in each compound. Three terminal carbonyl groups are bonded to each iron atom in all three molecules. The bond distance between the Mo atom and the Fe atom in the triangular base is longer (2.802–2.844 Å) than the bonds between Mo and the square-base Fe atoms (2.735–2.768 Å), the former being comparable to the Mo–Fe bond distances observed in **1** and **2** (2.815–2.889 Å). The S–S bond distance in **8** [2.041(2) Å] is similar to that in $[Fe_2(CO)_6(\mu\text{-}S_2)]$[11] (2.011 Å). Likewise, the Se–Se bond distance in **5** [2.313(12) Å] is similar to that of $[Fe_2(CO)_6(\mu\text{-}Se_2)]$[12] [2.293(2) Å].

Although the exact mechanism of formation of compounds **5**, **6** and **8** is not established as yet, it involves the formal loss of one $Fe(CO)_3$ group from $[Fe_2(CO)_6(\mu\text{-}S_2)]$ or $[Fe_2(CO)_6(\mu\text{-}Se_2)]$ which is formed from $[Fe_2(CO)_6(\mu\text{-SSe})]$ while stirring with $[Mo(CO)_5(thf)]$ at room temperature, and the addition of one $Fe(CO)_3E_2$ group (E = S or Se) and $[Fe_2(CO)_6(\mu\text{-}S_2)]$ or $[Fe_2(CO)_6(\mu\text{-SSe})]$ respectively thus formed to one $Mo(CO)_4$ group. Formally, one $[Fe_2(CO)_6(\mu\text{-}E_2)]$ molecule undergoes cleavage of a Fe–Fe and two Fe–E bonds and the other $[Fe_2(CO)_6(\mu\text{-}S_2)]$ or $[Fe_2(CO)_6(\mu\text{-SSe})]$ molecule undergoes one Fe–Fe and one S–S or S–Se bond scissions, and there is an overall formation of

Table 3 Selected bond lengths (Å) and angles (°) for $[Fe_3Mo(CO)_{11}(\mu_3\text{-}S)(\mu_3\text{-}Se)(\mu\text{-}Se_2)]$ **5**

Mo–Fe(1)	2.844(11)	Se(1)–Se(2)	2.313(12)
Mo–Fe(2)	2.768(11)	Se(1)–Fe(1)	2.357(13)
Mo–Fe(3)	2.752(11)	Se(2)–Fe(1)	2.379(13)
Mo–Se(1)	2.581(10)	SSe(3)–Fe(2)	2.276(2)
Mo–Se(2)	2.581(9)	SSe(3)–Fe(3)	2.284(2)
Mo–SSe(3)	2.437(2)	SSe(4)–Fe(2)	2.274(2)
Mo–SSe(4)	2.492(2)	SSe(4)–Fe(3)	2.277(2)
Se(1)–Mo–Fe(1)	51.2(3)	Fe(2)–Mo–Fe(1)	144.6(4)
Se(2)–Mo–Fe(1)	51.7(3)	Fe(3)–Mo–Fe(1)	137.4(4)
Fe(3)–Mo–Fe(2)	76.5(3)	SSe(3)–Mo–Fe(1)	134.2(5)
SSe(3)–Mo–Fe(2)	51.4(5)	SSe(4)–Mo–Fe(1)	151.0(5)
SSe(3)–Mo–Fe(3)	51.8(4)	Se(1)–Mo–Se(2)	53.2(2)
SSe(4)–Mo–Fe(2)	50.9(4)	SSe(3)–Mo–SSe(4)	74.5(5)
SSe(4)–Mo–Fe(3)	51.2(4)	SSe(3)–Mo–Se(1)	87.5(5)
Se(1)–Mo–Fe(2)	133.4(4)	SSe(3)–Mo–Se(2)	89.7(5)
Se(1)–Mo–Fe(3)	95.7(4)	SSe(4)–Mo–Se(1)	146.7(5)
Se(2)–Mo–Fe(2)	100.0(3)	SSe(4)–Mo–Se(2)	150.7(4)
Se(2)–Mo–Fe(3)	133.9(4)		

Table 4 Selected bond lengths (Å) and angles (°) for $[Fe_3Mo(CO)_{11}(\mu_3\text{-}S)_2(\mu\text{-SSe})]$ **6**

Mo–Fe(1)	2.819(2)	SSe(1)–SSe(2)	2.275(2)
Mo–Fe(2)	2.735(2)	SSe(1)–Fe(1)	2.318(2)
Mo–Fe(3)	2.750(2)	SSe(2)–Fe(1)	2.355(2)
Mo–SSe(1)	2.556(2)	Fe(2)–S(1)	2.235(3)
Mo–SSe(2)	2.560(2)	Fe(2)–S(2)	2.265(3)
Mo–S(1)	2.450(3)	Fe(3)–S(1)	2.238(3)
Mo–S(2)	2.411(3)	Fe(3)–S(2)	2.261(3)
SSe(1)–Mo–Fe(1)	50.81(5)	Fe(2)–Mo–Fe(1)	137.29(6)
SSe(2)–Mo–Fe(1)	51.67(5)	Fe(3)–Mo–Fe(1)	144.92(6)
Fe(2)–Mo–Fe(3)	76.32(5)	S(1)–Mo–Fe(1)	151.66(8)
S(1)–Mo–Fe(2)	50.71(7)	S(2)–Mo–Fe(1)	133.93(8)
S(1)–Mo–Fe(3)	50.59(7)	SSe(1)–Mo–SSe(2)	52.82(5)
S(2)–Mo–Fe(2)	51.76(7)	S(2)–Mo–S(1)	74.08(9)
S(2)–Mo–Fe(3)	51.45(8)	S(1)–Mo–SSe(1)	146.51(8)
SSe(1)–Mo–Fe(2)	95.94(6)	S(1)–Mo–SSe(2)	150.79(8)
SSe(1)–Mo–Fe(3)	133.57(6)	S(2)–Mo–SSe(1)	87.54(8)
SSe(2)–Mo–Fe(2)	133.68(6)	S(2)–Mo–SSe(2)	89.54(8)
SSe(2)–Mo–Fe(3)	100.30(5)		

Table 5 Selected bond lengths (Å) and angles (°) for $[Fe_3Mo(CO)_{11}(\mu_3\text{-}S)_2(\mu\text{-}S_2)]$ **8**

Mo–Fe(1)	2.735(8)	S(3)–S(4)	2.041(2)
Mo–Fe(2)	2.757(8)	Fe(1)–S(1)	2.241(14)
Mo–Fe(3)	2.802(9)	Fe(1)–S(2)	2.266(14)
Mo–S(1)	2.453(13)	Fe(2)–S(1)	2.239(14)
Mo–S(2)	2.408(13)	Fe(2)–S(2)	2.258(14)
Mo–S(3)	2.448(14)	Fe(3)–S(3)	2.233(2)
Mo–S(4)	2.449(13)	Fe(3)–S(4)	2.247(2)
Fe(1)–Mo–Fe(2)	76.4(2)	S(3)–Mo–Fe(1)	97.1(4)
S(1)–Mo–Fe(1)	50.8(3)	S(3)–Mo–Fe(2)	132.8(4)
S(1)–Mo–Fe(2)	50.5(3)	S(4)–Mo–Fe(1)	132.7(4)
S(2)–Mo–Fe(1)	51.8(3)	S(4)–Mo–Fe(2)	101.7(4)
S(2)–Mo–Fe(2)	51.3(3)	S(2)–Mo–S(1)	73.9(4)
S(3)–Mo–Fe(3)	49.8(4)	S(3)–Mo–S(4)	49.3(5)
S(4)–Mo–Fe(3)	50.1(3)	S(3)–Mo–S(1)	147.9(5)
Fe(1)–Mo–Fe(3)	137.3(3)	S(2)–Mo–S(3)	87.6(5)
Fe(2)–Mo–Fe(3)	144.6(3)	S(4)–Mo–S(1)	152.2(5)
S(1)–Mo–Fe(3)	152.5(4)	S(2)–Mo–S(4)	89.6(4)
S(2)–Mo–Fe(3)	133.3(4)		

Table 6 Crystal data for $[Fe_4Mo(CO)_{14}(\mu_3\text{-}S)_2(\mu_3\text{-}Te)_2]$ **2** and $[Fe_3Mo(CO)_{11}(\mu_3\text{-}E)(\mu_3\text{-}E')(\mu\text{-}E'_2)]$ (E = S, E′ = Se or S; $E'_2 = Se_2$ **5**, SSe **6** or S_2 **8**)

	2	**5**	**6**	**8**
Formula	$C_{14}Fe_4MoO_{14}S_2Te_2$	$C_{11}Fe_3MoO_{11}SSe_3$	$C_{11}Fe_3MoO_{11}S_3Se$	$C_{11}Fe_3MoO_{11}S_4$
M	1030.8	840.54	746.74	699.84
Crystal size/mm	0.40 × 0.40 × 0.40	0.40 × 0.40 × 0.20	0.40 × 0.20 × 0.10	0.40 × 0.30 × 0.20
Crystal system	Orthorhomic	Monoclinic	Monoclinic	Monoclinic
Space group	$Pna2_1$	$P2_1/n$	$P2_1/n$	$P2_1/n$
a/Å	14.469(3)	10.896(2)	10.801(2)	10.7703(9)
b/Å	11.627(1)	17.538(1)	17.456(3)	17.630(1)
c/Å	15.473(3)	11.667(1)	11.594(3)	11.609(2)
β/°		108.93(1)	108.85(3)	108.49(1)
U/Å^3	2603.1(4)	2108.9(4)	2068.6(10)	2090.5(3)
Z	4	4	4	4
D_c/g cm^{-3}	2.630	2.647	2.398	2.224
μ(Mo-Kα)/cm^{-1}	50.65	79.30	47.68	30.77
F(000)	1912	1568	1424	1352
T/K	298(2)	298(2)	247(2)	298(2)
θ Range/°	2.25–24.98	2.18–22.50	2.19–22.50	2.18–22.50
hkl Ranges	−1 to 17, −1 to 13, −18 to +1	−1 to 11, −1 to 18, −12 to +12	−1 to 11, −1 to 18, −12 to +12	−1 to 11, −1 to 18, −12 to +12
Reflections collected	3060	1496	3464	3496
Independent reflections	2561	2760	2705	2732
R_{int}	0.0435	0.0327	0.0397	0.0247
Data, restraints, parameters	2558, 1, 335	2760, 0, 274	2702, 0, 273	2732, 0, 271
Goodness of fit on F^2	1.515	1.085	1.231	1.127
Final *R* indices [$I > 2\sigma(I)$]*	0.0353	0.0328, 0.0713	0.0428, 0.1031	0.0301, 0.0702
(all data)	0.0858	0.0466, 0.0731	0.0704, 0.1191	0.0399, 0.0748
Largest difference peak and hole/e Å^{-3}	0.934, −0.707	0.622, −0.726	1.117, −0.816	0.482, −0.467

* $R = \Sigma||(F_o - F_c)|/\Sigma F_o$; $wR2 = \Sigma w(F_o^2 - F_c^2)^2/\Sigma[w(F_o^2)^2]^{\frac{1}{2}}$.

seven new bonds, three Fe–Mo, one S–Mo and three E–Mo. Both the sulfur and selenium ligands adopt the μ_3 bridging mode in **5**, **6** and **8** and thereby function as four-electron donors to the clusters.

Experimental

General procedures

All reactions and manipulations were performed using standard Schlenk techniques under an atmosphere of prepurified dry argon. Solvents were purified, dried and distilled under an argon or nitrogen atmosphere prior to use. Infrared spectra were recorded on a Nicolet Impact 400 FT spectrometer as hexane solutions in 0.1 mm path length NaCl cells. Elemental analyses were performed on a Carlo-Erba automatic analyser. The compounds $[Fe_2(CO)_6(\mu\text{-}EE')]$ [13] (E = S or Se; E′ = S, Se or Te) and $[Mo(CO)_5(thf)]$ [14] were prepared by established procedures; $[Mo(CO)_6]$ was obtained from Aldrich Chemical Co. and used as such. Photochemical reactions were carried out in a water-cooled double-walled quartz vessel having a 125 W immersion-type mercury lamp manufactured by Applied Photophysics Ltd.

Typical preparation of $[Fe_4Mo(CO)_{14}(\mu_3\text{-}E)_2(\mu_3\text{-}E')_2]$ (E = S or Se; E′ = S, Se or Te) and $[Fe_3Mo(CO)_{11}(\mu_3\text{-}E)(\mu_3\text{-}E')(\mu\text{-}E'_2)]$ (E = S; E′ = Se or Te; E = E′ = S, Se)

Conditions used for the preparation of compounds **1**–**10** and yields of products are summarised in Table 1. In a typical preparation, a thf solution (120 cm^3) of $[Mo(CO)_6]$ (0.26–0.72 mmol) was irradiated with 366 nm UV light in an immersion-type photolysis instrument for 10 min under a constant argon purge. The yellow-green thf solution of $[Mo(CO)_5(thf)]$ was added to a hexane solution (50 cm^3) containing $[Fe_2(CO)_6(\mu\text{-}EE')]$, (E = S or Se; E′ = S, Se or Te) (0.51–1.45 mmol). The reaction mixture was stirred at room temperature for 3 h. The solvent was removed *in vacuo*, and the residue subjected to chromatographic work-up on a silica gel column. Using hexane as eluent, the following bands were obtained, in order of elution: $[Mo(CO)_6]$ (trace), previously reported maroon band of $[Fe_2Mo(CO)_{10}(\mu_3\text{-}E)(\mu_3\text{-}E')]$ {EE′ = SeTe, 0.045 g, 9%, based on $[Fe_2(CO)_6(\mu\text{-}SeTe)]$ consumed; STe, 0.02 g, 8%, based on $[Fe_2(CO)_6(\mu\text{-}STe)]$ consumed; Se_2, 0.1 g, 20%, based on $[Fe_2(CO)_6(\mu\text{-}Se_2)]$ consumed}, unchanged $[Fe_2(CO)_6(\mu\text{-}EE')]$ (EE′ = SeTe, 40; STe, 34; SSe, 37; S_2, 40; Se_2, 50%), a green band of $[Fe_4Mo(CO)_{14}(\mu_3\text{-}E)_2(\mu_3\text{-}E')_2]$ and an orange band of $[Fe_3Mo(CO)_{11}(\mu_3\text{-}E)(\mu_3\text{-}E')(\mu\text{-}E'_2)]$.

X-Ray crystallography

Dark red crystals of compounds **2**, **5**, **6** and **8** were grown by layering hexane on their dichloromethane solutions and slow evaporation of the solvents at −5 °C. Suitable crystals were selected and mounted on thin glass fibres with epoxy cement. Crystal data and structure refinement details are given in Table 6. The data were measured on a Siemens P4 diffractometer using graphite-monochromated Mo-Kα radiation (λ = 0.710 73 Å). The unit-cell parameters were obtained by least-squares refinement of the angular settings of 24 reflections ($20 \leqslant 2\theta \leqslant 25°$). Preliminary photographic data indicated an orthorhombic crystal system for **2** and a monoclinic crystal system for **5**, **6** and **8**. The systematic absences in the diffraction data are consistent with either $Pna2_1$ or *Pnma* for **2**, and uniquely $P2_1/n$ for **5**, **6** and **8**. The *E* statistics suggested the non-centrosymmetric option for **2**. Solution and refinement in $Pna2_1$ produced a plane defined by Fe(1), Fe(2), S(2) and Te(2) that is nearly perpendicular to the crystallographic *z* axis. If the atoms S(1) and Te(1) were disordered, this plane would constitute a molecular mirror plane. However, the results of refinement strongly support the non-centrosymmetric alternative for these reasons: bond distances and angles fall into narrow and expected ranges, no positional element in the correlation matrix exceeds 0.5, and the isotropic equivalent thermal parameters for S(1) (0.035) and Te(1) (0.038) are nearly equal when refined as pure elements. Similarly, no compositional disorder is seen at the S(2) and Te(2) sites. The structures were solved by direct methods, completed by subsequent Fourier-difference syntheses and refined by full-matrix least-squares procedures. Semiempirical absorption corrections were applied. All non-hydrogen atoms were refined with anisotropic displacement coefficients. Hydrogen atoms were treated as idealised contributions. Two of

the chalcogen atoms in **5** and **6** were found to be statistically disordered over two positions with an occupancy distribution of 70:30 and 75:25 respectively. This disorder was modelled by refining the occupancies of the chalcogen atoms which were arbitrarily identified as selenium atoms [labelled as SSe(3) and SSe(4) in **5**; SSe(1) and SSe(2) in **6**]. All software and sources of the scattering factors are contained in the SHELXTL (5.3) program library.[15] Final cycles of refinement converged at R and R' values listed in Table 2.

CCDC reference number 186/601.

References

1 P. Mathur, D. Chakrabarty and I. J. Mavunkal, *J. Cluster Sci*., 1993, **4**, 351; P. Mathur, I. J. Mavunkal and A. L. Rheingold, *J. Chem. Soc., Chem. Commun*., 1989, 382.
2 D. A. Lesch and T. B. Rauchfuss, *Inorg. Chem*., 1983, **22**, 1854.
3 P. Mathur, D. Chakrabarty, Md. M. Hossain, R. S. Rashid, V. Rugmini and A. L. Rheingold, *Inorg. Chem*., 1992, **31**, 1106.
4 P. Mathur, P. Sekar, C. V. V. Satyanarayana and M. F. Mahon, *J. Chem. Soc., Dalton Trans*., 1996, 2173.
5 P. Mathur and P. Sekar, *Chem. Commun*., 1996, 727.
6 C. K. Johnson, ORTEP, Report ORNL-5138, Oak Ridge National Laboratory, Oak Ridge, TN, 1976.
7 B. Cowans, J. Noordik and M. R. DuBois, *Organometallics*, 1983, **2**, 931.
8 F. Richter and H. Vahrenkamp, *Chem. Ber*., 1982, **115**, 3243.
9 L.-C. Song, J.-Y. Shen, Q.-M. Hu and X.-Y. Huang, *Organometallics*, 1995, **14**, 98.
10 P. D. Williams, M. D. Curtis, D. N. Duffy and W. M. Butler, *Organometallics*, 1983, **2**, 165.
11 C. H. Wei and L. F. Dahl, *Inorg. Chem*., 1965, **4**, 1.
12 C. F. Campana, F. Y.-K. Lo and L. F. Dahl, *Inorg. Chem*., 1979, **18**, 3060.
13 P. Mathur, D. Chakrabarty and Md. M. Hossain, *J. Organomet. Chem*., 1991, **401**, 167; P. Mathur, P. Sekar, C. V. V. Satyanarayana and M. F. Mahon, *Organometallics*, 1995, **14**, 2115.
14 W. J. Schlientz and J. K. Ruff, *Inorg. Chem*., 1972, **11**, 2265.
15 G. M. Sheldrick, Siemens XRD, Madison, WI, 1996.

Received 8*th April* 1997; *Paper* 7/02408H